DOI: 10.35840/2631-5076/9260

VIBGYOR ePress

International Journal of
Metallurgy and Metal Physics

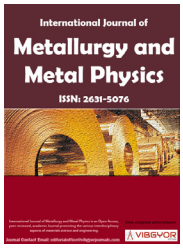

ISSN: 2631-5076

Microstructure and Properties of Tungsten Rhenium Alloy Prepared by Laser Sintering

Shan Jiang*

College of Materials Science and Engineering, Chongqing University of Arts and Sciences, P. R. China

Abstract

Tungsten alloy with addition of rhenium and tantalum was prepared by laser sintering. Microstructure and properties of the samples were tested by optical microscope, X-ray diffractometer and microhardness tester. Dense tungsten alloy block materials were prepared by adjusting laser beam power and laser spot scanning speed. The oxidation of powder can be avoided by desorption and deoxygenation pretreatment and inert gas protection. Static recrystallization occurred in the laser sintering process. In the core of the sample, equiaxed grains significantly larger than the powder particles were formed. In the edge of the sample, where the temperature was lower than the core due to heat dissipation, small and immature equiaxed grains whose size was close to the particle size of the powder were formed. The addition of tantalum and rhenium formed a solid solution in tungsten. Because of the effect of solid solution atoms to the lattice, with the increase of the addition of tantalum and rhenium, the density of samples decreased, while the microhardness increased accordingly.

Keywords

Tungsten, Alloys, Laser, Sintering, Cladding

Introduction

Tungsten and its alloys are widely used in aerospace, nuclear power, ships, automobiles, electronics, electrical, chemical and many other fields [1-4]. Tungsten belongs to rare metals, and the content of tungsten on the earth is only 0.001%. Therefore, how to use tungsten with high quality has become the focus of new technology researches [5-7]. At present, the research direction of developing high-grade tungsten products with high technology content and high added value includes deep cemented carbide manufacturing, high precision and high performance functionally gradient cemented carbide, alloy of precision die and wear-resistant parts, super-thin and super-large tungsten sheet, etc. [8,9]. Tungsten, as a traditional lighting material, has a weakness that its seismic performance is poor, so it can not meet the needs of use in harsh vibration environment. Therefore, other elements are usually added to tungsten to improve its toughness. Tungsten, tantalum and rhenium are all high melting point metals. Among all metals, tungsten has the highest melting point (3410 °C), followed by rhenium (3180 °C and tantalum (2995 °C). Ta and Re have moderate hardness, ductility and good mechanical properties [10]. In this paper,

***Corresponding author:** *Shan Jiang, College of Materials Science and Engineering, Chongqing University of Arts and Sciences, Chongqing, 402160, P. R. China*

Accepted: October 21, 2020; **Published:** October 23, 2020

ISSN 2631-5076

Luo et al. Int J Metall Met Phys 2020, 5:059

Citation: Jiang S (2020) Microstructure and Properties of Tungsten Rhenium Alloy Prepared by Laser Sintering. Int J Metall Met Phys 5:060

tungsten-based alloys are prepared by adding a small amount of rhenium and tantalum into tungsten matrix, which can improve the ductility of materials without significantly reducing their melting point, thus forming alloys with high melting point and good ductility. Because of the high melting point of tungsten-based alloys, it is impossible to produce tungsten-based alloys by traditional casting methods. At present, the production process of tungsten products has roughly gone through three processes: Vertical melting, thermal deformation and mechanical cutting to produce final products. Vertical melting sintering includes mixing, honeying, pressure forming, catalytic degreasing or solvent degreasing, sintering and so on. Generally speaking, the current production process of tungsten products mainly has the following problems: Long process, post-treatment of pollutants, difficult recycling of cutting materials, and difficult preparation of products with complex shape. In this context, tungsten-based alloy bulk materials were prepared by laser sintering, which provided theoretical and experimental support for 3D printing technology of tungsten products. The so-called laser sintering is the use of ultra-high energy density laser beam (10^4-10^5W/cm^2) as a heat source to irradiate the material surface, so that the material melts, diffuses and solidifies rapidly, thus forming a material with special properties [11-15]. Compared with vertical melting sintering, laser technology has the following advantages: Short cycle, pollution-free, and can prepare complex products. However, one of the key problems in the preparation of metal materials by laser sintering is the oxidation of powders and the density of sintered materials. This paper will focus on these technical difficulties.

Experimental Procedure

The tungsten powder (average particle size approximately 3 μm), tantalum powder (average particle size approximately 15 μm) and tantalum powder (average particle size approximately 15 μm) were used as ingredients according to the mass ratio in Table 1. The prepared raw materials were placed in a ball mill with a volume of 2 L. The ball mill was lined with stainless steel, and anhydrous ethanol was used as a process control agent. The amount of the material was 25% of the total mass of the powder. After ball milling for 10 h, the mixed powder was cleaned 3 times using anhydrous ethanol, put into a centrifuge for separation and then put into a vacuum drying box for drying and desorption. The drying box was set to 120 °C and the drying time was 6 h. The dried mixed powder was stored in a drying bottle for backup. The mixed powder was put into a laser powder delivery device and sintered using coaxial powder method under argon protection. The laser head has a square spot of 4 × 4 mm^2, and the laser scanning speed is 5 mm/s. The sintering power of the laser was set at 1.6~1.8 kW. The laser sintered sample was processed into a square specimen of uniform shape for subsequent characterization test. The morphology of the powder was characterized by Noval 400 scanning electron microscope (SEM), under 20 kV, with a working distance of 20 mm and a tilt angle of 70°. Metallographic observation was performed on the sample. The ratio of metallogenic corrosion fluids was: distilled water 40g, potassium ferricyanide 8g, sodium hydroxide 8g, and corrosion time was 30s. The XRD analysis was conducted using a Rigaku D/MAX-2500V diffractometer with Cu Kα radiation λ = 1.5406 Å operated at 40 kV. The hardness test was conducted with an HRD-150 tester with the load of 200g and holding time 10s.

Table 1: Ratio of tungsten, rhenium and tantalum in the powder.

Samples\Mass (%)	W	Re	Ta
1	96	3	1
2	93	6	1
3	90	9	1

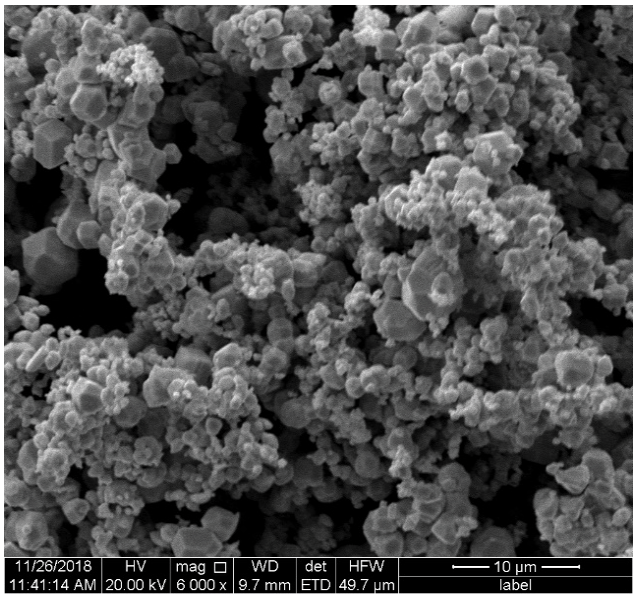

Figure 1: Scanning electron microscopic photograph.

Results and Discussion

Morphological characterization of powders

The powder of specimen 1 after ball milling was observed by SEM. The morphology and size of the powder were shown in Figure 1. It can be seen from the figure that tungsten powder particles, which accounted for the absolute majority of mass and volume, had an isoaxial shape and a uniform particle size distribution. The vast majority of particle sizes were concentrated at 2~4 μm and the maximum particle size was about 5 μm. The initial particle size of rhenium and tantalum particles was about 15 ~20 μm, and the shape was also irregular. However, after ball milling, the large size grains were not seen, indicating that the ball milling had a significant crushing effect on the powder and tantalum powder.

Metallographic characterization of block

Figure 2 shows the microstructure of the microstructure of the tungsten alloy prepared. The grain boundaries of all three samples were relatively straight, and the shape of the grain formed by the straight grain boundary was close to equiaxed grains. Most of the crystal boundaries were smooth and clear, indicating that the alloy formed by laser sintering had good crystallinity and tightness. In Figure 2a, Figure 2b and Figure 2c, different textures of grains can be found. For example, in Figure 2a and Figure 2c, black spots can be found inside the grains. In Figure 2b, there was a significant difference in color depth due to the different orientation distribution of the grains. This was mainly due to the different degree of corrosion of different orientation grains during the corrosion process. This shows that the orientation distribution of grains was random and the microstructure formed was homogeneous. From Figure 2b it can be seen that there were cracks in the grain boundaries. There are two possible reasons for this kind of cracks: One is that there was a rapid thermal contraction during the laser sintering process that caused the grain boundary in the area to be pulled apart, and the other is that the grain boundary bond strength decreased due to the appearance of oxide impurities. This problem needs to be improved in subsequent experiments. In Figure 2d, in the edge area

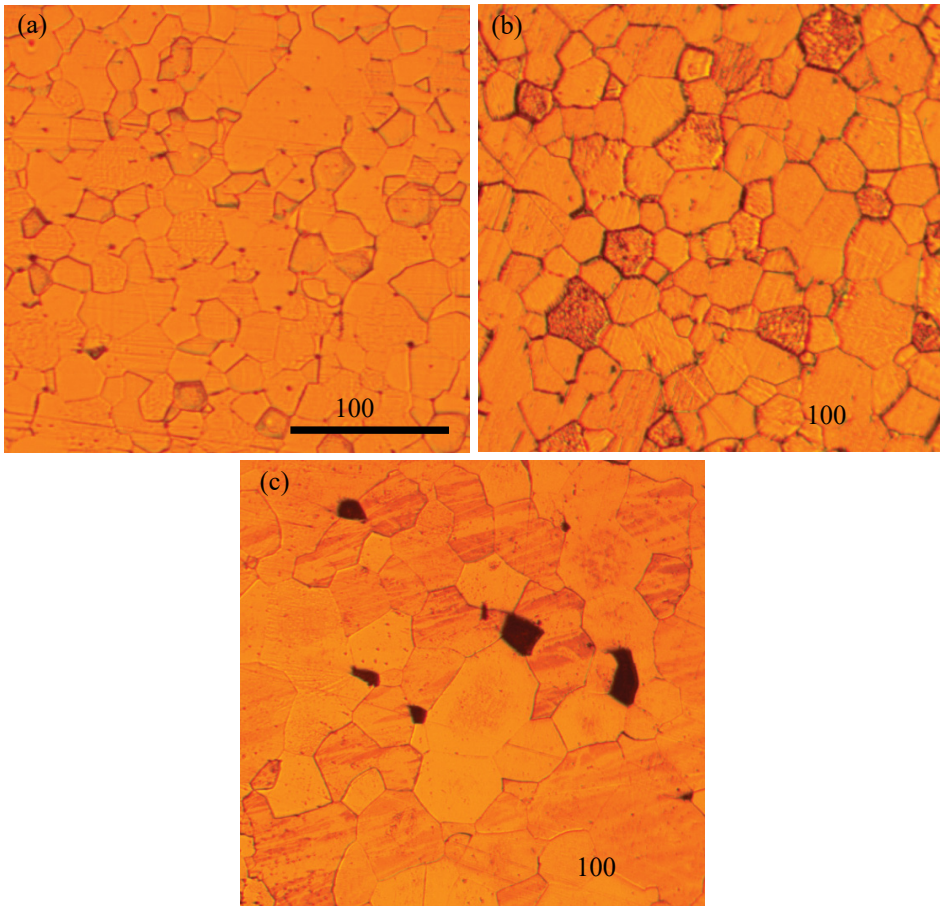

Figure 2: (a, b and c) are metallographic micrographs of the core of sample 1, 2 and 3, respectively.

of the specimen, due to insufficient sintering, some small isaxial grains appear, and the average grain size is only about 5~10 μm. This shows that this part could not grow up after the crystalline core on the surface of the sample because of the fast loss of heat. From Figure 2a, it can be seen that the average grain size was about 21 μm, the average grain size in Figure 2b was about 39 μm, and the average grain size in Figure 2c was about 52 μm. In a summary, the addition of tantalum inhibited the growth of grains, and the grain size decreased with the increase of tantalum addition.

XRD analysis of blocks

The chemical abstracts service (CAS) of tungsten is 7440-33-7, and α-W is a body-centered cubic structure. Each cell contains 2 metal atoms. Cell parameters: a = b = b = 316.52 pm, α = β = γ = 90°. The atomic number of rhenium is 73, adjacent to tungsten, belongs to the sixth cycle VB group element in the elemental cycle system, CAS is 7440-25-7, and the crystal structure is the same body-centered cubic structure. Each cell contains 2 metal atoms. Cell parameters: a = b = b = 330.13 pm, α = β = γ = 90°. According to the XRD test principle, the crystal can be used as an X-ray grating, and the coherent scattering generated by the lattice will interfere with the light, thereby increasing or weakening the intensity of the scattered X-rays. According to the Bragg equation ($2d\sin\vartheta = n\lambda$, where d is the crystal plane spacing, ϑ is the angle between the incident Ray, λ is the wavelength, and n is the reflection series), for X-ray diffraction, when the optical path difference is equal to an integer multiple of the wavelength, the scattered rays of the crystal surface will be strengthened. At this time, the diffraction peak of the corresponding crystal surface will be generated in the XRD patterns.

Since the crystal types and cell parameters of tungsten and tantalum are very close, the characteristic peaks generated in the XRD test are also very close. However, due to the small amount of tantalum in this experiment, the peak strength is obviously low. Figure 3 shows the XRD patterns of powder and laser sintered blocks for samples 1, 2 and 3, respectively. As shown in the Figure 3, in all curves the three strong peaks of tungsten can be clearly observed. At the same time in the powder curves of the three specimens, except the characteristic peaks of tungsten, other peaks are too weak to be observed. However, for the block samples, the characteristic peaks of Re_3W and ReW appeared. In addition, it can be clearly seen that with the increase of addition of Re, the intensity of these peaks was enhanced significantly. This shows that Re have not a good solid solution in tungsten. To make Re enter the lattice of tungsten to form a displacement solid solution, solid solution treatment must be conducted.

Density and hardness testing of block

In order to investigate the physical properties of the samples, the density of each sample was tested by drainage method. As shown in Figure 4, the densities of samples 1, 2 and 3 are 18.86, 19.05 and 19.13 g/cm^3, respectively. Because the atomic mass

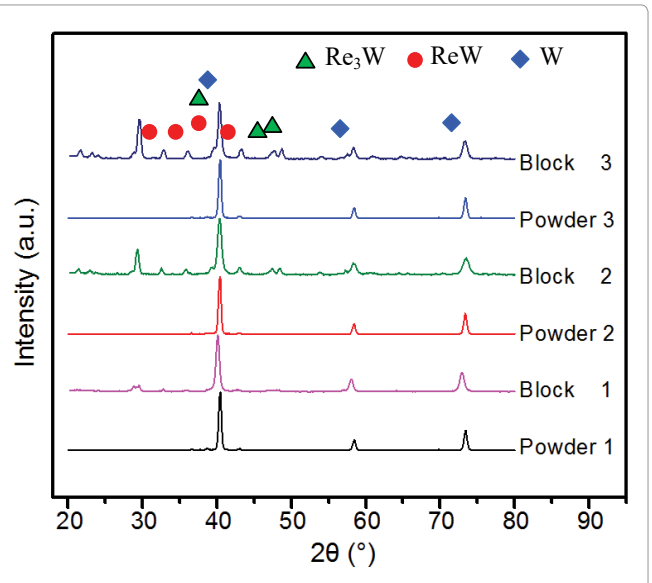

Figure 3: XRD patterns of powder and bulk of samples.

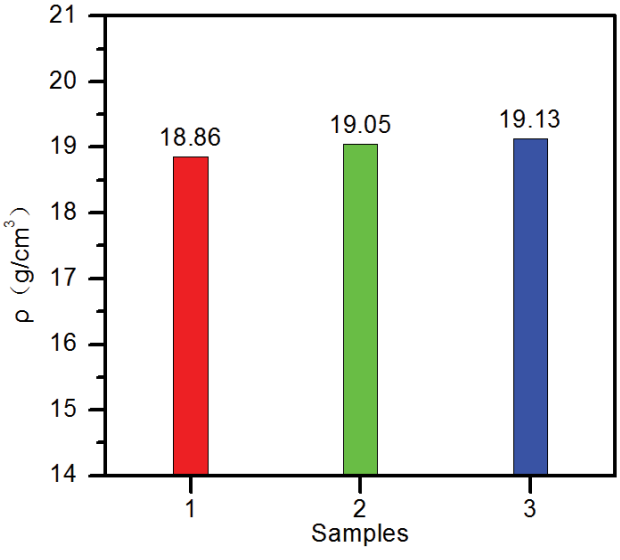

Figure 4: Density of the samples.

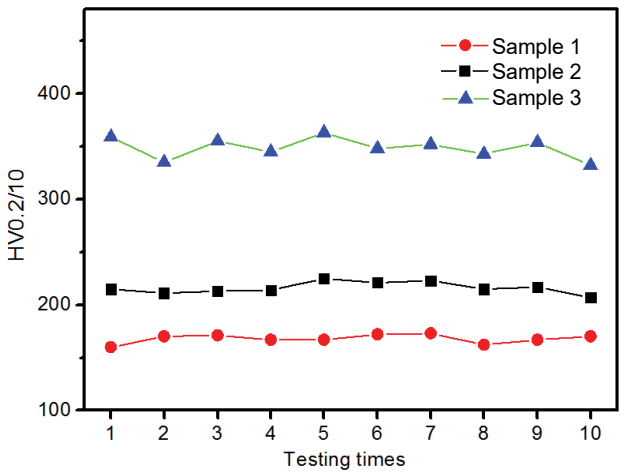

Figure 5: Microhardness of the samples.

of tungsten, tantalum and rhenium are 183.84, 180.95 and 186.21, and the densities of which are 19.25, 16.68 and 21.04 g/cm^3, respectively, the addition of Re into the tungsten will increase the density while the addition of tantalum will reduce the density.

Meanwhile, the Vickers hardness of the samples was also tested. As shown in Figure 5, the average microhardness of samples 1, 2 and 3 were 167.1HV0.2/10, 218.5HV0.2/10 and 345.6HV0.2/10, respectively. Comparing the density and microhardness of the sample, it is found that the order of hardness from high to low is sample 1, 2 and 3, consistent with the order of density. Therefore, it can be concluded that the microhardness increases with the density. The main reason is that as a result of the strengthening effect of the second phase, the dislocation movement was hindered by the appearance of the second phase, so the strength of the material was enhanced. With the increase of the second phase, the strengthening effect became more and more remarkable. Therefore, with the increase of rhenium content, the hardness value increased with the increase of the second phase content.

Conclusions

In this paper, tungsten-based alloys with tantalum and rhenium were prepared by laser sintering, and their structures and properties were tested. The following conclusions were obtained:

1) From the point of view of preparation technology, powder oxidation can be avoided by inert gas protection. Dense tungsten alloy bulk materials can be prepared by adjusting laser beam power and laser spot scanning speed.

2) Static recrystallization occurred during laser sintering, and equiaxed grains were formed in the core of the sample, which were larger than those of the powder particles. The grain size of the three samples decreased with the increase of rhenium content.

3) The addition of rhenium forms an intermetallic compounds. With the increase of the amount of rhenium, both the amount of intermetallic compounds and the density of the samples increased accordingly.

Acknowledgments

This work is supported by the National Natural Science Foundation of China (Grant no. 51301215), Science and Technology Research Program of Chongqing Municipal Education Commission(KJQN201801314 and KJQN201801306), and Chongqing Science and Technology Commission Project (cstc2019jcyj-msxmX0601, cstc2018jcyjAX0472 and cstc2015jcyjA70014).

References

1. UR Kiran, S Venkat, B Rishikesh, VK Iyer, M Sankaranarayana, et al. (2013) Effect of tungsten content on microstructure and mechanical properties of swaged tungsten heavy alloys. Mater Sci Eng A 582: 389-396.
2. UR Kiran, M Sankaranarayana, GVS Nageswara Rao, TK Nandy (2017) Effect of cobalt addition on microstructure and mechanical properties of tungsten heavy alloys. T Indian Metals 70: 615-622.
3. Z Wu, Y Zhang, CM Yang, QJ Liu (2014) Mechanical properties of tungsten heavy alloy and damage behaviors after hypervelocity impact. Rare Metals 33: 414-418.
4. NN Qiu, Y Zhang, C Zhang, H Tong, XP Song (2018) Tensile properties of tungsten-rhenium wires with nanofibrous structure. International Journal of Minerals Metallurgy and Materials 25: 77-81.
5. KH Lee, SI Cha, HJ Ryu, SH Hong (2007) Effect of two-stage sintering process on microstructure and mechanical properties of ods tungsten heavy alloy. Mater Sci Eng A 458: 323-329.
6. Y Ma, P Yue, W Liu, J Zhang (2013) Microstructure and dynamic mechanical properties of extruded tungsten alloy rods by microwave sintering. Rare Metal Mat Eng 42: 1362-1366.
7. M Scapin (2015) Mechanical characterization and modeling of the heavy tungsten alloy IT180. Int J Refract Met H 50: 258-268.

8. SJ Bless, K Tarcza, R Chau, E Taleff, C Persad (2006) Dynamic fracture of tungsten heavy alloys. Int J Impact Eng 33: 100-108.

9. SF Moustafa, SH Kaitbay, GM Abdo (2010) Liquid-phase sintering of tungsten heavy alloys. Defect Diffus Forum 303-304: 55-62.

10. C Deng, SF Liu, JL Ji, XB Hao, ZQ Zhang, et al. (2014) Texture evolution of high purity tantalum under different rolling paths. J Mate Process Tech 214: 462-469.

11. DZ Wang, QW Hu, XY Zeng (2015) Influences of parameters on microstructures and mechanical properties of $Cr_{13}Ni_5Si_2$ based composite coating by laser induction hybird cladding. Surf Coat Tech 280: 359-369.

12. L He, Y Tan, X Wang, Q Jing, X Hong (2015) Tribological properties of laser cladding TiB_2 particles reinforced Ni-base alloy composite coatings on aluminum alloy. Rare Metals 34: 789-796.

13. H Qin, ZH Cai, P Zhang, Z Yang (2014) Development status of laser cladding technologies. Appl Mech Mater 584-586: 1500-1503.

14. AI Noskov, AK Gilmutdinov, RM Yanbaev (2017) Effect of coaxial laser cladding parameters on bead formation. Int J Min Met Mater 24: 550-556.

15. H Duan, X Liu, X Ran, J Li, D Liu (2017) Mechanical properties and microstructure of 3D-printed high Co-Ni secondary hardening steel fabricated by laser melting deposition. Int J Min Met Mater 24: 1027-1033.

ISSN 2631-5076

DOI: 10.35840/2631-5076/9260

Citation: Jiang S (2020) Microstructure and Properties of Tungsten Rhenium Alloy Prepared by Laser Sintering. Int J Metall Met Phys 5:060